Planar channeling in superlattices: Theory

J. A. Ellison
Department of Mathematics, University of New Mexico, Albuquerque, New Mexico 87131

S. T. Picraux
Sandia National Laboratories, P.O. Box 5800, Albuquerque, New Mexico 87185-5800

W. R. Allen and W. K. Chu
Department of Physics and Astronomy, University of North Carolina, Chapel Hill, North Carolina 27514
(Received 30 March 1987; revised manuscript received 6 October 1987)

The well-known continuum model theory for planar channeled energetic particles in perfect crystals is extended to layered crystalline structures and applied to superlattices. In a strained-layer structure, the planar channels with normals which are not perpendicular to the growth direction change their direction at each interface, and this dramatically influences the channeling behavior. The governing equation of motion for a planar channeled ion in a strained-layer superlattice with equal layer thicknesses is a one degree of freedom nonlinear oscillator which is periodically forced with a sequence of δ functions. These δ functions, which are of equal spacing and amplitude with alternating sign, represent the tilts at each of the interfaces. Thus upon matching an effective channeled particle wavelength, corresponding to a natural period of the nonlinear oscillator, to the period of the strained-layer superlattice, corresponding to the periodic forcing, strong resonance effects are expected. The condition of one effective wavelength per period corresponds to a rapid dechanneling at a well-defined depth (catastrophic dechanneling), whereas two wavelengths per period corresponds to no enhanced dechanneling after the first one or two layers (resonance channeling). A phase plane analysis is used to characterize the channeled particle motion. Detailed calculations using the Moliere continuum potential are compared with our previously described modified harmonic model, and new results are presented for the phase plane evolution, as well as the dechanneling as a function of depth, incident angle, energy, and layer thickness. General scaling laws are developed and nearly universal curves are obtained for the dechanneling versus depth under catastrophic dechanneling.

I. INTRODUCTION

Rutherford backscattering analysis of energetic particle channeling in superlattices has recently led to the observation of a new channeling phenomenon.[1-3] Furthermore, it has led to new techniques to measure the strain in these structures,[4-13] which is the subject of a recent review.[14] Strained-layer superlattices consist of alternating layers of two materials of similar crystal structure with lattice constants which have a lattice mismatch of the order of 1%. Thus under commensurate growth, for example by molecular-beam epitaxy (MBE) or metalorganic chemical-vapor deposition (MOCVD) epitaxy, these structures have alternating compressive and tensile strained built into the layers. These artificially modulated semiconducting materials, called strained-layer superlattices (SLS's), have interesting new electro-optic properties.[15]

Three channeling methods to study SLS structures have been examined. The basis of these measurements is the fact that the planar and axial directions undergo slight alternating tilts along all crystal directions inclined to the growth direction; these tilts are of the order of the critical angle for channeling (0.1° to 1°). The first two methods involve axial channeling, one being the measurement of the rate of dechanneling of the beam along axial directions[4,7,10,11] and the other being the measurement of angular scans with respect to axial directions.[5,6,9,12,13] A third technique involves the measurement of the planar dechanneling under a resonance condition, referred to as catastrophic dechanneling. Strong dechanneling occurs after the beam passes through a few superlattice layers, in this case due to a matching of the effective channeled particle wavelength with the superlattice period.[1] This latter technique is made particularly sensitive by measuring the angular dependence of the depth of catastrophic dechanneling.[2] Of these three techniques the planar channeling approach provides the greatest sensitivity to the measurement of small strain. Lattice mismatches ≈ 0.1 to 0.5% can be detected with good sensitivity. Also the planar resonance effect introduces a new channeling phenomenon, and raises questions of interest from the basic viewpoint of atomic collision studies in solids.

Here we present the general theory for planar channeling in layered structures and apply it to strained-layer superlattices. We will develop the theory within the continuum model[16-20] framework for energetic planar-channeled particles. This model is valid, for example, for He ions with energies greater than ~ 500 keV. A more general theory for channeling in crystals with nonstraight channels was briefly discussed in a previous work on dechanneling by dislocations[21] in terms of an arbitrary curvature function. However, the specialized case of layered structures with straight channels within each layer

and tilts in the channel direction at each interface provides for some particularly fascinating behavior. The governing equation of motion for strained-layer superlattices is a one degree of freedom nonlinear oscillator which is forced with a periodic forcing function of an impulsive nature representing the tilt at each interface. Thus one expects resonance effects to play an important role when the natural frequencies are near the forced frequencies. In this model transverse energy is conserved in each layer; thus we do not include electronic or nuclear multiple scattering or other effects which lead to a nonconservation of transverse energy of the particles with increasing depth. The continuum approximation is particularly good for catastrophic dechanneling conditions in SLS's, since the depth region of interest is relatively near the surface, within the first few planar channeled particle wavelengths. We emphasize that while the present theory is discussed in detail for strained-layer superlattices of equal-layer thickness, it can be applied to any strained-layer system involving one or more layers. This application may be valuable for future planar channeling studies, for example, in single-strained quantum wells and other heteroepitaxial systems with one or more strained layers present.

In this paper we first present the basic theoretical framework for channeled particle trajectory motion in a layered structure. Calculations of channeled particle motion are then carried out for a static Moliere potential with a dechanneling criteria based on a minimum impact parameter of the Thomas-Fermi screening distance from the planes. The results are compared to our previous modified harmonic model (MHM), which gives good physical understanding of the planar channeling resonance phenomena. We then discuss how a phase plane analysis of the planar channeled particle transverse position and momentum distribution as a function of depth gives valuable insight into the resonance dechanneling behavior. Two types of resonances are discussed: catastrophic dechanneling which gives a maximum in the rate of dechanneling when the effective channeled partial wavelength matches the superlattice period, and resonance channeling which gives a minimum dechanneling with depth when the effective wavelength equals one half the period. Dechanneling-versus-depth results are then presented for both conditions, and the importance of the angular dependence of the incident beam is discussed for the case of catastrophic dechanneling. Finally we develop scaling laws for planar channeling in strained-layer superlattices and present a set of nearly universal curves for catastrophic dechanneling as a function of normalized depth and strain angle.

This theory paper is the first of a sequence of papers in which we will discuss planar channeling in strained-layer superlattices.[22–24]

II. PLANAR CHANNELING THEORY

A. Continuum model

We begin by presenting that theoretical framework for the continuum model[16,20] needed to extend channeling theory from the perfect crystal to layered structures. When an energetic particle beam enters a crystal at a small angle with respect to a set of crystal planes, the collective atomic potentials steer the particles back and forth between the planes. The motion of a nonrelativistic particle is governed by the Hamiltonian

$$H=\frac{1}{2m}(p_x^2+p_y^2+p_z^2)+V(x,y,z)\ , \tag{1}$$

where V is a periodic potential reflecting the crystal symmetry and taken to be the sum of screened Coulomb potentials with the lattice atoms fixed at the perfect crystal lattice sites. This model includes the effects of electrons only to the extent that they screen the nucleus of the lattice atoms; it does not contain the scattering or energy loss of a channeled particle due to the individual electrons. Also, this model does not contain the effect of the thermal motion of the lattice atoms. In general, these effects cannot be ignored; however, it is H which is primarily responsible for the particle motion; thermal vibrations, electron multiple scattering, and energy loss can be treated as perturbations. In our case, we can ignore energy loss and electron multiple scattering to a good approximation, since we are dealing with very shallow depths into the crystal. The effect of thermal vibrations can be incorporated into the continuum model in a zeroth-order way as discussed later and in a forthcoming paper.[23]

The crystal planes are taken to be parallel to the y-z plane. Because the energetic channeled particles are moving fast and nearly parallel to this plane, the potential of Eq. (1) can to good approximation be averaged over the y-z plane. This is called the planar continuum model[16–20] and $U(x)$ will denote this averaged, continuum model, potential. For heavy particles of MeV energies (i.e., protons and larger) classical mechanics applies. Clearly, the y and z momenta are conserved and without loss of generality we assume $p_y=0$; hence, the equations of motion become

$$m\frac{d^2x}{dt^2}+U'(x)=0,\quad m\frac{d^2z}{dt^2}=0\ . \tag{2}$$

Since the z velocity v_z is constant, $z=v_z t$ can be taken as the independent variable which gives

$$\frac{d^2x}{dz^2}+\frac{1}{2E_z}U'(x)=0\ , \tag{3}$$

where $E_z=\frac{1}{2}mv_z^2$. Furthermore, planar channeling only occurs for angles less than the characteristic angle

$$\psi_p=(2\pi Z_1 Z_2 e^2 N\, d_p a_T/E)^{1/2}\ , \tag{4}$$

and this angle is small (e.g., for 1.2-MeV He along the {110} planes of GaP $\psi_p=0.39°$); thus the incident particle energy E and the energy E_z are nearly identical for channeling and we replace E_z by E. In the above equation, Z_1 is the atomic number of the incident particle, Z_2 the average atomic number of the target crystal planes, N is the density of atoms in the crystal, d_p is the interplanar distance, and $a_T=0.8853a_0(Z_1^{1/2}+Z_2^{1/2})^{-2/3}$, where $a_0=0.529$ Å is the Bohr radius.

The most commonly used atomic potential in Eq. (1) for the purpose of channeling is the Moliere approxima-

tion to the Thomas-Fermi potential, namely,

$$V(r)=\frac{Z_1Z_2e^2}{r}\sum_{i=1}^{3}\alpha_i\exp\left[\frac{-\beta_i r}{a_T}\right], \tag{5}$$

where $\alpha=\{0.1,0.55,0.35\}$, $\beta=\{6.0,1.2,0.3\}$, and a_T is the Thomas-Fermi screening length. The Moliere continuum potential for a single atomic plane, obtained by averaging the potential in Eq. (1) over the plane, is then

$$V_{ps}(\rho)=E\psi_p^2\sum_{i=1}^{3}\left[\frac{\alpha_i}{\beta_i}\right]\exp-\left[\frac{\beta_i\rho}{a_T}\right], \tag{6}$$

where ψ_p is defined in (4) and ρ is the distance from the plane.[17] An approximate correction for the thermal vibration of the lattice atoms may be included by convoluting the continuum potential as a whole with the probability distribution for the vibrating atoms. For the Moliere case, inclusion of thermal averaging gives

$$V_{pt}(\rho)=E\psi_p^2\sum_{i=1}^{3}\frac{1}{2}\left[\frac{\alpha_i}{\beta_i}\right]e^{\tau_i}\left\{e^{-\beta_i\rho/a_T}\operatorname{erfc}\left[\frac{1}{\sqrt{2}}\left[\frac{\beta_i u_1}{a_T}-\frac{\rho}{u_1}\right]\right]+e^{\beta_i\rho/a_T}\operatorname{erfc}\left[\frac{1}{\sqrt{2}}\left[\frac{\beta_i u_1}{a_T}+\frac{\rho}{u_1}\right]\right]\right\}, \tag{7}$$

where $\tau_i=(\beta_i u_1/\sqrt{2}a_T)^2$. In the derivation of (7) it is assumed that the individual atoms vibrate independently and that in each translational degree of freedom the probability density of the displacement is normal with mean zero and variance u_1^2. Other atomic potentials that have been used include the Lindhard approximation to the Thomas-Fermi potential[17] and the Doyle-Turner potential[25] which is based on a Hartree-Fock calculation for isolated atoms. The Doyle-Turner potential has recently been shown to be quite accurate in channeling radiation studies[26] with electrons and positrons, and it will be compared with the Moliere potential and experimental results in a forthcoming paper.[23]

For the full planar continuum potential U needed to describe the motion of a particle in a channel, we sum the contributions from the two adjacent planes, giving

$$U(x)=V_p\left[\frac{d_p}{2}-x\right]+V_p\left[\frac{d_p}{2}+x\right]-2V_p\left[\frac{d_p}{2}\right], \tag{8}$$

where x is measured from the midpoint between the planes and U has been adjusted so that $U(0)=0$. Four planes would be more accurate but this is a negligible correction here. The Moliere and thermally averaged Moliere potentials as defined by (6)–(8) are shown in Fig. 1 for He ions incident on the {110} planes of $GaAs_xP_{1-x}$ with $x=0.075$. In order to illustrate the theory of channeled particle motion in a SLS we need to choose a specific case. We have chosen equal layer thicknesses of $GaP/GaAs_xP_{1-x}$ with $x=0.15$. Since changes in interplanar spacing and planar potentials are negligible from layer to layer we use the average composition in our calculations. The insert shows the contribution from individual planes as given by Eq. (6). In analytical analyses of planar channeling, a harmonic approximation $U(x)\simeq\frac{1}{2}\alpha x^2$ to Eq. (8) is sometimes used. This is also shown in Fig. 1 where α has been chosen to match the static Moliere potential a short distance from the plane. The harmonic model gives a number of the qualitative proper-

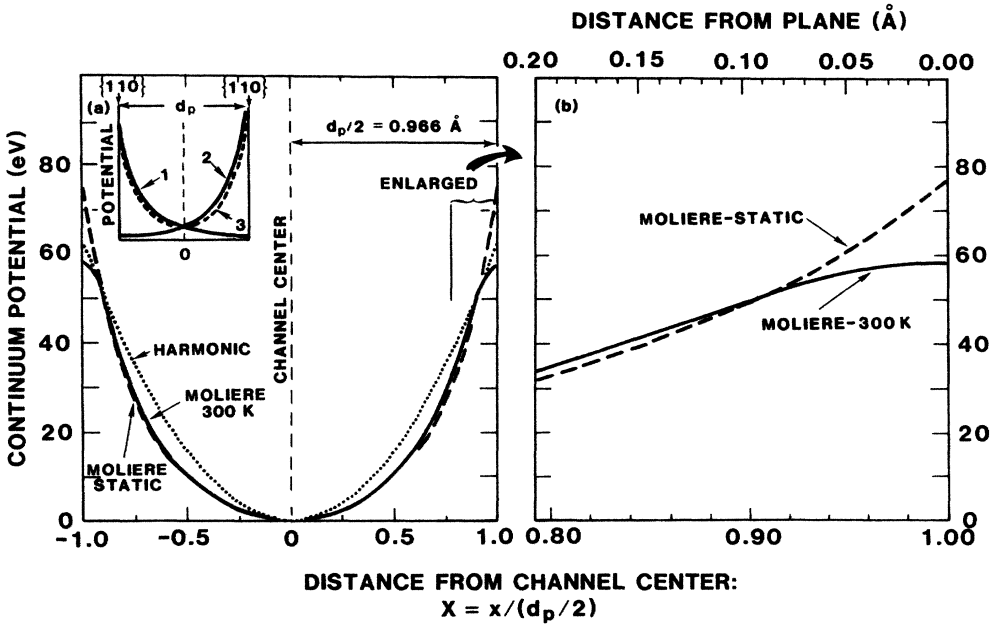

FIG. 1. Various continuum potentials for planar channeling of He ions incident along the {110} planes of $GaAs_xP_{1-x}$ with $x=0.075$. The dotted curve is for a harmonic potential, the dashed curve is for the static Moliere potential, and the solid curve is for the 300 K thermally averaged Moliere potential. Enlargement of the figures near the {110} plane is also given.

ties of planar channeling, but in general it is not a good approximation for quantitative analysis.

The equation of motion for channeled particles given in (3) has the conservation law

$$E_\perp = E\left[\frac{dx}{dz}\right]^2 + U(x) , \tag{9}$$

$E_\perp$ is commonly called the transverse energy, and the fact that $E_\perp$ is constant along solutions $x(z)$ of Eq. (3) is easily seen by differentiating Eq. (9) with respect to z and making use of Eq. (3). For channeling trajectories, the angle ψ the path $x(z)$ makes with the z axis is $0(\psi_p)$, also ψ_p is small and $\psi \simeq \tan\psi = dx/dz$. Therefore, in the following we take $\psi = dx/dz$. Equation (9) defines a one-parameter family of concentric ovals in the (x,ψ) phase plane as $E_\perp$ varies, thus the solutions of Eq. (3) are periodic. The wavelength of the periodic trajectories as a function of $E_\perp$ is given by

$$\lambda(E_\perp) = 4\sqrt{E}\int_0^a \frac{dx}{\sqrt{E_\perp - U(x)}} , \tag{10}$$

where a is the amplitude of the motion defined implicitly by

$$U(a) = E_\perp . \tag{11}$$

The wavelength for 1.2-MeV He in {110} $GaAs_xP_{1-x}$, $x=0.075$ for the Moliere potential is shown in Fig. 2 as a function of both $E_\perp$ and normalized amplitude $A = a/(d_p/2)$ and can be obtained from the universal curves for determining λ as a function of amplitude given in Ref. 18. Notice that λ is a monotone decreasing function, which is characteristic of channeling potentials, because the closer a positive particle moves to a plane, the harder it is pushed away by the positive nuclei of the lattice atoms. Thus channeling potentials are hard spring-type potentials, in contrast to, for example, the pendulum equation which has a soft spring potential. Furthermore, it is important to note that knowing $\lambda(E_\perp)$ is equivalent to knowing $U(x)$ since $\lambda(E_\perp)$ uniquely determines $U(x)$ from its inverse by

$$x(U) = \frac{1}{4\pi\sqrt{E}}\int_0^U \frac{\lambda(E_\perp)}{\sqrt{U - E_\perp}} dE_\perp . \tag{12}$$

This is discussed in Refs. 18 and 27 and has been used by Gibson and Golovchenko[28] to examine the potential from measurements of λ. The difference between the harmonic and Moliere potentials is much more apparent in Fig. 2 than in Fig. 1. This is true in general, so that it is much easier to compare and contrast different potentials by looking at the wavelength function rather than the potential itself. The arrows in Fig. 2 show how to use λ versus A and λ versus $E_\perp$ to determine the potential, that is, choosing $A = 2a/d_p$ gives $\lambda(A)$ and $\lambda(E_\perp)$ which gives $E_\perp = U(a)$. For the thermally averaged potential (not shown), λ decreases to a minimum near the thermal vibration amplitude and then increases to infinity as the amplitude approaches $d_p/2$.

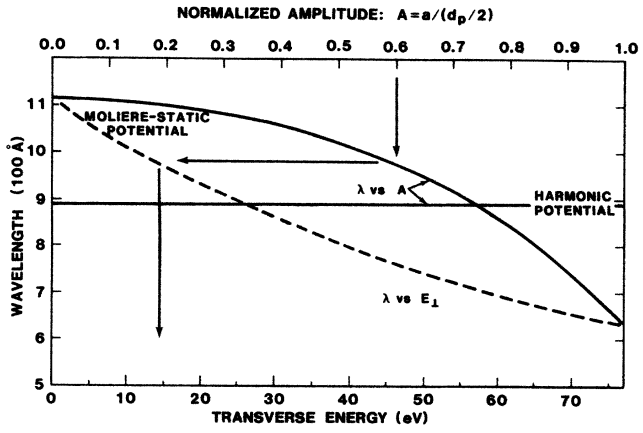

FIG. 2. Wavelength for 1.2-MeV He in {110} $GaAs_xP_{1-x}$, $x=0.075$, as a function of normalized amplitude (solid curve) and as a function of transverse energy (dashed curve) for the Moliere static potential. The arrows indicate a way to determine $E_\perp$ given A. For example, $A=0.6$ corresponds to $\lambda=975$ Å, which corresponds to $E_\perp = 14.4$ eV. The harmonic potential of Fig. 1 for 1.2-MeV He gives $\lambda=880$ Å independent of A or $E_\perp$.

The phase plane portrait in the (x,ψ) plane for the channeled particle motion provides a convenient means to follow the evolution of an ensemble of channeled particles as they penetrate a crystal. In Fig. 3(a), we show several phase plane ovals defined by Eq. (9) for the Moliere potential with the largest oval corresponding to a particle with the maximum transverse energy, $E_{\perp c}$, defined by $E_{\perp c} = U(x_c)$, where x_c is defined as a critical distance such that particles are dechanneled if they approach the planes more closely than this value. In Fig. 3 we have chosen $x_c = d_p/2 - a_T$ for illustrative purposes. The x,ψ axes are normalized by x_c and ψ_c, where these are related by

$$E_{\perp c} = E\psi_c^2 = U(x_c) . \tag{13}$$

The value of ψ_c is typically on the order of ψ_p. As each planar-channeled particle moves through the crystal, it moves clockwise on the oval defined by its transverse energy with wavelength given by Eq. (10) (see also Fig. 2). If we consider a beam incident on a crystal with an angle ψ_0 with respect to the planes and uniformly distributed in space then it appears as a horizontal line labeled 0 in the phase lane as shown in Fig. 3(b). In Fig. 3(b) we have ignored those particles with $E_\perp > E_{\perp c}$. As the beam moves through the crystal, the line begins to spiral as shown in the figure for depths of $z=74$, 148, and 222 Å. The particles on the outer ovals have a larger average angular velocity than those on the inner ovals because λ is a monotone decreasing function of $E_\perp$. As the beam evolves, these spirals become wound tighter, eventually giving rise to a coarse grain statistical equilibrium distribution.[29] For a harmonic potential the angular velocity is constant and the phase flow curves will remain straight lines. Particle trajectories $x(z)$, for the case of Fig. 3(b) are shown in Fig. 3(c) and one can see that typical quarter wavelengths are on the order of 200 Å, consistent with Fig. 2.

B. Modified harmonic model

The phase flow curves of Fig. 3(b) and the sample paths of Fig. 3(c) must be obtained by the numerical integration of Eq. (3). In our early work on superlattices, we wanted an analytical/geometrical procedure for following the phase flow. We first used a harmonic potential $U(x)=\frac{1}{2}\alpha x^2$ and tried to adjust the parameter α to obtain agreement with experiment, but this one-parameter approach did not give satisfactory results. We then developed what we call the modified harmonic model (MHM) which allows for separate but simple approximations to $x(z)$ and $\psi(z)$.

The MHM is obtained as an approximation to the full model of Eqs. (3) and (9) by first defining a critical distance x_c such that particles are dechanneled if they approach the planes more closely than this value. This defines a critical transverse energy $E_{\perp c}$ and a critical angle ψ_c by Eq. (13). Our *first* approximation replaces the phase place ovals defined by Eq. (9) by the ellipses

$$\left[\frac{\psi(z)}{\psi_c}\right]^2+\left[\frac{x(z)}{x_c}\right]^2=\left[\frac{\psi_0}{\psi_c}\right]^2+\left[\frac{x_0}{x_c}\right]^2, \tag{14}$$

where $x(0)=x_0$ and $\psi(0)=\psi_0$. One can see that the ellipse with right-hand side equal to 1 goes through the points $(0,\psi_c)$ and $(x_c,0)$, so that this ellipse is a good approximation to the oval of Eq. (9) with $E_\perp=E_{\perp c}$. From Figs. 3(a) and 3(a') one can see that other ovals are somewhat less well approximated. Our *second* approximation takes the phase plane rotation rate to be a fixed value of $2\pi/\lambda_e$, where λ_e is an effective wavelength parameter to be determined. Note that distances along the channel convert to rates through the particle velocity $v_z=\sqrt{E/2m}$ along the channel. With these two approximations $x(z)$ and $\psi(z)$ can be written

$$\frac{x(z)}{x_c}=\frac{x_0}{x_c}\cos\left[\frac{2\pi}{\lambda_e}z\right]+\frac{\psi_0}{\psi_c}\sin\left[\frac{2\pi}{\lambda_e}z\right], \tag{15a}$$

$$\frac{\psi(z)}{\psi_c}=-\frac{x_0}{x_c}\sin\left[\frac{2\pi}{\lambda_e}z\right]+\frac{\psi_0}{\psi_c}\cos\left[\frac{2\pi}{\lambda_e}z\right]. \tag{15b}$$

Here we have two free parameters, the wavelength λ_e and the dechanneling parameter x_c. The other parameter ψ_c is determined from (13). We choose x_c to be the same as in the full model and choose λ_e to approximate the phase flow in the full model.

Equations (15) cannot be obtained by approximating $U(x)$ by a harmonic potential. This is because in the harmonic model $\psi(z)=dx(z)/dz$ which implies from Eq. (15) that $\lambda_e=2\pi x_c/\psi_c$. However, in the MHM x_c and λ_e are chosen independently and in general do not satisfy this relation. It is because of this distinction that we call this model the modified harmonic model. Also, this illustrates an important aspect of thinking in terms of the phase plane, namely, it facilitates separate approximations for $x(z)$ and $\psi(z)$.

The MHM is illustrated in Fig. 3. Figure (3b') shows the phase flow of the particles. Notice that the initial line remains straight, because of the second approximation which fixed the phase plane rotation rate. Also notice that the rotation rate has been chosen so that the straight line approximates in an average way the Moliere phase flow line of Fig. 3(b). The trajectories in Fig. 3(c') are drawn using Eq. (15a), with $\lambda_e=888$ Å. It is of interest to note that for the Moliere potential $\lambda=888$ Å corresponds to a normalized amplitude of approximately 0.75 as is seen from Fig. 2. In a practical situation λ_e can be chosen by computing the wavelength function from Eq. (10) and picking an appropriate λ or from a backscattering experiment as mentioned in Sec. IV B.

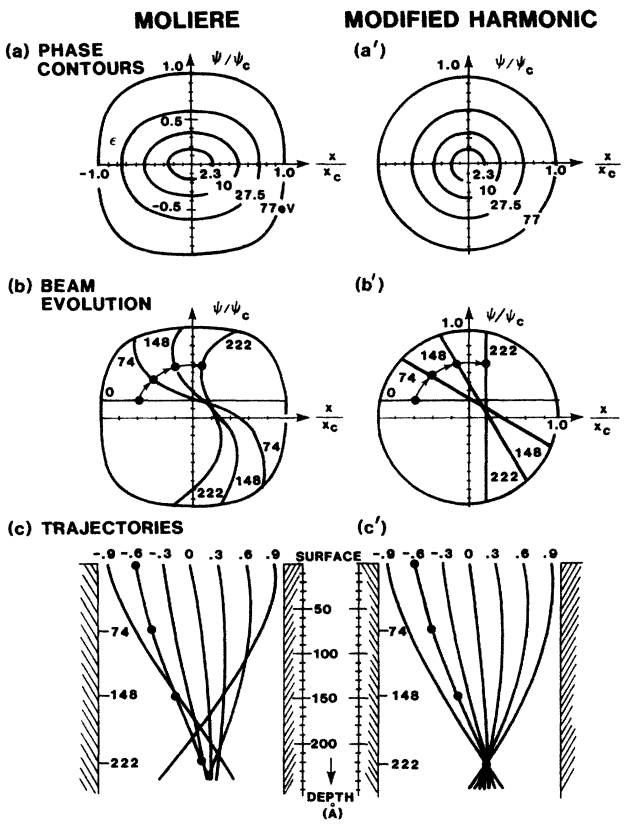

FIG. 3. Calculations based on Moliere potential for 1.2-MeV He ions in simple crystal $GaAs_xP_{1-x}$, $x=0.075$ are shown on the left-hand side. (a) *Potential contours.* (b) *Phase flow* at depths of 74, 148, and 222 Å. Black dots refer to the motion of a single projectile. (c) *Trajectories* for projectiles at several initial conditions. On the right, [(a'), (b'), (c')], the calculations are based on modified harmonic model (MHM). Potential contours simplify into circles, phase flow reduces to a rotating straight line, and a well-defined focus is evident for the trajectories.

III. PLANAR CHANNELING THEORY IN SLS

A. Continuum model

In a strained-layer superlattice planar channels inclined to the growth normal are no longer straight, but are made up of straight segments of planes of fixed length s. We refer to s as the path length per layer, it is related

to the layer thickness through the cosine of the angle between the normal and inclined directions. At each interface, along these planes, the planar direction changes alternately by $\pm\Delta\psi$ (in lattice-matched superlattices $\Delta\psi=0$). The situation is shown schematically in Fig. 4. Thus in each segment the motion evolves according to Eq. (3) and since the coordinate frame changes at each interface, the angle of a trajectory with respect to the planes has a jump discontinuity of $\pm\Delta\psi$ at each interface. Thus, the equation of motion [Eq. (3)] becomes

$$\frac{d^2x}{dz^2}+\frac{1}{2E}U'(x)=\sum_{j=1}(-1)^j\Delta\psi\,\delta(z-js)\ , \tag{16}$$

where δ denotes the Dirac delta function. Integrating Eq. (16) from js^- to js^+ gives

$$\psi(js^+)-\psi(js^-)=(-1)^j\Delta\psi\ ,$$

consistent with the superlattice structure of alternating $\pm\Delta\psi$ tilts at each interface. Here we have used the small-angle assumption so that $\psi=dx/dz$. By convention, we take the first angular change to be negative.

Equation (16) is written for equal path lengths per layer s, but clearly it is easily written for any other layer combination. Hence it can be applied to any strained-layer system involving one or more layers. In fact these cases can be viewed as a limiting situation of the more general theory of channeling in curved crystal planes which was developed in a study of the effect of dislocations on channeling motions.[21] In that case the equations of motion are defined by the Lagrangian

$$L(\dot{x},\dot{z},x,z)=\tfrac{1}{2}m\{\dot{x}^2+[1+x\kappa(z)]^2\dot{z}^2\}-U(x)\ ,$$

where $\kappa(z)$ is the curvature of the planes as a function of the distance z down the channel. In the case of the SLS the curvature is just the right-hand side of Eq. (16).

A spatially uniform beam incident at an angle ψ_0 with respect to the first set of planes can be represented by a horizontal line as shown in Fig. 3(b). Here a positive ψ_0 means in the direction that the second set of planes tilt relative to the first set of planes (first layer). The phase flow of this line evolves just as is shown in Fig. 3 in the first layer. Then at the first interface all particles are moved down by $\Delta\psi$ in the phase plane. The phase flow then evolves according to Eq. (3) until it comes to the second interface, at which depth all particles are moved up by $\Delta\psi$. This process continues and a particle is said to be dechanneled if it comes within a critical distance of approach to the planes $|x(z)|\geq x_c$. This defines the dechanneled fraction of the beam at a depth z as a function of E, ψ_0, $\Delta\psi$, and s. Because for typical channeling potentials Eq. (3) must be solved numerically, we calculate the dechanneled fraction by numerically integrating Eq. (16) for a large number of initial x positions x_0 keeping track of the depth at which each particle becomes dechanneled.[30,31] This contains all the necessary theoretical information to describe particle channeling in strained-layer structures. For the calculations in this paper, we take for the alternating layers $GaAs_xP_{1-x}/GaP$, $x=0.15$, use a static Moliere potential based on an average of the two layers take the critical distance for channeling $x_c=d_p/2-a_T$, and assume equal path lengths per layer of $s=444$ Å for the superlattice. Also we take $d_p=1.9322$ Å which is the average interplanar spacing for GaP and $GaAs_{0.15}P_{0.85}$ and $a_T=0.1375$ Å. The potential and wavelength functions are thus shown in Figs. 1 and 2.

Our calculation gives the spatial density $\rho(x;z)$ of channeled particles at a depth z with a sharp cutoff in channeling at $x=x_c$.[32] A more exact treatment would introduce a probability for a particle being dechanneled given it is at position x and then compute the dechanneled fraction as the integral over ρ. Our approach is consistent with not including multiple scattering effects and gives the essential physics of channeling in superlattices.

Equation (16) is a nonlinear oscillator with a periodic forcing term, and so one expects nonlinear resonance effects. In fact, because the forcing term is a periodic delta function this is the simplest type of equation for the study of nonlinear resonance. Various other types of forcing functions, both periodic and nonperiodic, would result for other strained-layer structures, and our approach is easily extended to such cases. The forced nonlinear oscillator has a rich literature and Ref. 33 contains references that may be of interest in the present context of Eq. (16).

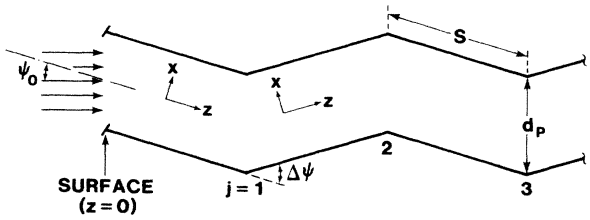

FIG. 4. Schematic representation of an inclined {110} planar channel of a {100} SLS. The x-z frame of reference is set by the channel direction in each SLS layer; thus the reference frame is rotated at each interface. The dimension is significantly enlarged relative to our planar spacing ($d_p=1.9322$ Å), tilt angle ($\Delta\psi=0.15°$), and beam incident angle ($-2°<\psi_0<2°$) as compared with the path length per layer of the SLS ($s=444$ Å) along the inclined {110} channels.

B. Modified harmonic model

The extension of the MHM to the strained-layer superlattice is straightforward. Once x_c (and thus ψ_c) and λ_e are chosen then the angular rotation, $\theta=2\pi s/\lambda_e$ of the phase flow line in each layer and the jump $\pm\Delta\psi/\psi_c$ of the phase flow line at each interface are determined. Thus the MHM leads to a very simple geometrical picture. The initial straight line is rotated clockwise θ units, moved down $\Delta\psi/\psi_c$ at the first interface, rotated clockwise θ units and moved up $\Delta\psi/\psi_c$ at the second interface, rotated θ units and moved down $\Delta\psi/\psi_c$ at the third interface, and so on (see Figs. 5 and 6). As before, a particle is dechanneled if its position x reaches $\pm x_c$. Because of this simplicity, analytical formulas for the dechanneled fraction at a depth z as a function of λ_c, ψ_0,

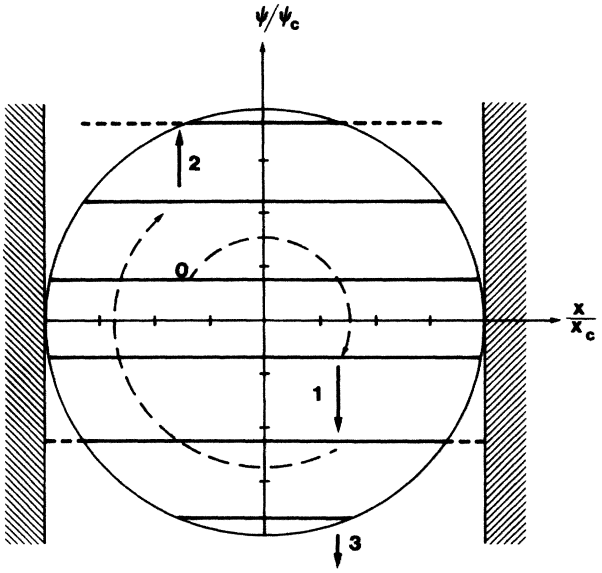

FIG. 5. Phase flow in the phase plane based on the MHM for the *catastrophic dechanneling* condition where the impulse occurs at every π rotation and the half wavelength equals the path length per layer ($\lambda/2=s$). Maximum dechanneling occurs.

$\Delta\psi$, and s are easily determined for special values of θ as shown in Sec. IV. Notice that $\Delta\psi/\psi_c$ controls the degree of dechanneling per layer for a given rotation. Thus the proper choice of ψ_c is important for numerical estimates.

IV. RESONANCE PHENOMENA IN THE MHM

Since the periodic structure of the SLS provides an angular impulse at each interface, as given in Eq. (16), resonance effects might be anticipated for those particles whose unforced frequencies are close to the forcing frequency. The MHM gives a simple qualitative framework and geometric interpretation for understanding and predicting the motion of planar-channeled particles in a SLS near such resonances. It indicates that matching half the effective wavelength λ_e with the path length per layer gives $\theta=2\pi s/\lambda_e=\pi$ which corresponds to a maximal rate of dechanneling. We call this condition *catastrophic dechanneling*. In contrast, matching the effective wavelength with the path length per layer gives $\theta=2\pi$, which corresponds to the minimal dechanneling and is called *resonance channeling*. More generally, catastrophic dechanneling occurs for $(n-\frac{1}{2})\lambda_e=s$ and resonance channeling occurs for $n\lambda_e=s$, where n is a positive integer. We will elaborate these two resonance phenomena in this section for $n=1$, since they have been observed in our experiments.

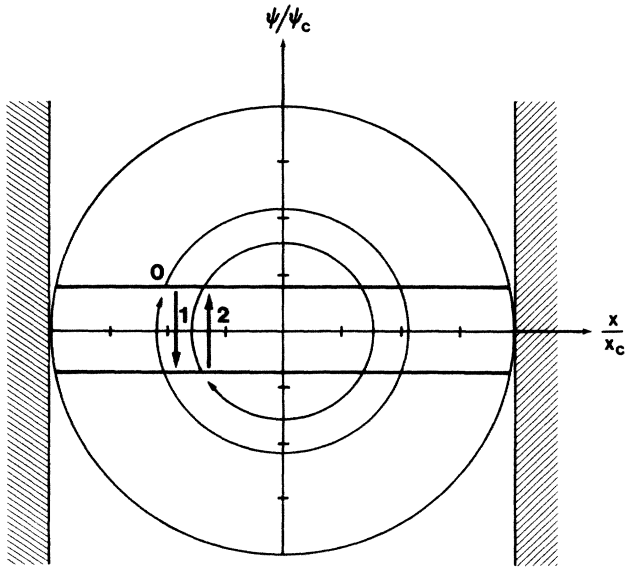

FIG. 6. Same as Fig. 5 for the resonance channeling condition where the impulse occurs at every 2π rotation and the wavelength equals the path length per layer ($\lambda=s$). Maximum channeling occurs.

A. Connection between different resonance conditions

Resonance has a number of technical meanings in both mathematics and physics. At this point we are using the term loosely to mean an enhancement; thus the resonance phenomenon of catastrophic dechanneling is an enhancement in the rate of dechanneling whereas resonance channeling is an enhancement in the fraction of channeled particles.

In the context of the MHM, catastrophic dechanneling is closely related to the phenomena of linear resonance in differential equations where the forcing period is equal to the natural period of oscillation. The classic example of such resonance behavior is the harmonically forced simple harmonic oscillator: $\ddot{x}+\omega_1^2 x=F\cos\omega_2 z$, where the amplitude of the response is proportional to $(\omega_1^2-\omega_2^2)^{-1}$ which becomes unbounded as $\omega_2\rightarrow\omega_1$. While this illustrates the type of behavior seen in catastrophic dechanneling, it does not contain the features of resonance channeling. To see how both these phenomena can arise in a linear model we consider Eq. (16) in the approximation $U'(z)=\alpha x$ and with the special initial condition $x(0)=\psi(0)=0$. A simple calculation shows that the phase plane coordinates just after the nth interface $z=ns^+$ are

$$\begin{aligned} x(ns^+)&=\frac{\Delta\psi}{\omega}\sum_{j=1}^{n}(-1)^j\sin[(n-j)\omega s]\ , \\ \psi(ns^+)&=\Delta\psi\sum_{j=1}^{n}(-1)^j\cos[(n-j)\omega s]\ , \end{aligned} \tag{17}$$

where $\omega^2=\alpha/2E$ and $n=1,2,\ldots$. From Eqs. (9) and (17) we find

$$\begin{aligned} \frac{E_\perp(n)}{E}&=\psi^2+\omega^2x^2\,|_{z=ns^+} \\ &=\Delta\psi^2\begin{cases} n^2, & \cos(\omega s)=-1 \\ \dfrac{1+(-1)^{n+1}\cos(n\omega s)}{1+\cos(\omega s)}, & \cos(\omega s)\neq -1\ . \end{cases} \end{aligned} \tag{18}$$

This clearly shows the usual resonance phenomenon with

$E_\perp(n)$ growing with the square of n for $\cos(\omega s)=-1$. If we let $A(n,\theta)=E_\perp(n)/E(\Delta\psi)^2$ with $\theta=\omega s$ then it can be shown that the least-upper bound of the function $A(n,\theta)$ over n is

$$A(\theta):=\operatorname*{lub}_{n\geq 1}\{A(n,\theta)\}=\begin{cases}\dfrac{1+\cos\left[\dfrac{2\pi}{4m+3}\right]}{1+\cos\theta}\dfrac{\theta}{2\pi}=\dfrac{p}{4m+2}, & m=1,2,\ldots\\ \dfrac{2}{1+\cos\theta}, & \text{otherwise},\end{cases}\tag{19}$$

where p is an integer. Since $\cos(2\pi/4m+2)$ is close to 1 for $m\neq 1$, $A(\theta)=2/(1+\cos\theta)$ for all practical purposes. Thus the least-upper bound for the transverse energy $E_{\perp s}$ of particle $x_0=\psi_0=0$ as a function of superlattice layer thickness s is given by

$$\frac{E_{\perp s}}{E(\Delta\psi)^2}=\frac{2}{1+\cos(\omega s)}\,.\tag{20}$$

Since in the SLS case we are usually interested in the channeling over the first few layers, we show in Fig. 7 the normalized value of the transverse energy for the maximum taken over the first five layers. Except for the dip near $\theta=\frac{2}{3}\pi$ and $\frac{4}{3}\pi$ this curve is nearly indistinguishable from Eq. (20); thus the convergence is very rapid.

To better understand Fig. 7, assume that the energy E and potential coefficient α are fixed and that the SLS tilt angle $\Delta\psi=\frac{1}{2}\psi_c$, where the critical transverse energy for channeling is $E_{\perp c}=E\psi_c^2$. The horizontal dashed line is $E_{\perp s}=E_{\perp c}=4E(\Delta\psi)^2$ and so when A_5 is below the dashed line in Fig. 7 the transverse energy of the particle with initial coordinates $x=\psi=0$ has not exceeded the critical transverse energy $E_{\perp c}$. In contrast, there are values of the SLS path length per layer s such as for θ near π and 3π where the function has exceeded this critical transverse energy at one of the first five interfaces so that the particle has been dechanneled. This response curve therefore shows the usual linear resonance phenomena of unbounded solutions, which we associate with the catastrophic dechanneling. However, it also has two new features, namely, a minimum in the response curve which we associate with resonance channeling and a periodicity in the maxima and minima which corresponds to multiple wavelengths within superlattice layers. In Secs. V and VI, we will discuss these resonance conditions in the nonlinear model, here we further discuss them in the MHM.

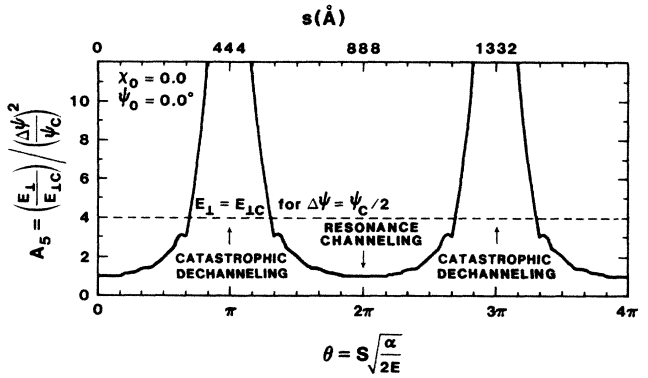

FIG. 7. Calculated maximum value of the normalized transverse energy over the first five layers of a SLS for a particle entering the crystal at $x_0=\psi_0=0$ vs the rotation θ per layer on the phase plane which depends on the path length per layer s. The dashed line corresponds to the critical transverse energy, $E_{\perp c}=E\psi_c^2$, for channeling for the case of a SLS tilt angle $\Delta\psi=\psi_c/2$. Based on a harmonic potential and Eqs. (17)–(20).

B. Catastrophic dechanneling

The MHM predicts a catastrophic dechanneling for $\theta=\pi$ as illustrated in Fig. 5. The beam is incident on the crystal planes with an angle of $\psi_0=+(\Delta\psi)/2$ and is uniformly distributed over $(-d_p/2,d_p/2)$ as shown by the horizontal line labeled 0 in Fig. 5. As the particles move through the first layer, the phase line rotates through an angle π as it comes to the first interface (lines labeled 1). At this interface, the horizontal phase flow line moves vertically from $-(\Delta\psi)/2$ to $-3(\Delta\psi)/2$. The horizontal line then rotates through an angle π in the next layer to $\psi=3(\Delta\psi)/2$, and the interface changes the angular coordinate from $3(\Delta\psi)/2$ to $5(\Delta\psi)/2$. The next rotation and impulse moves all particles out of the phase circle and thus they will become dechanneled as they rotate into the planes at $x=-x_c$ in this layer. Therefore for $\theta=\pi(\lambda_e/2=s)$, we have a constructive reinforcement which moves the particles out of the channeled beam as rapidly as possible. The MHM thus suggests this as an interesting case to investigate both theoretically in the nonlinear model and experimentally.

Experimentally an effective planar-channeled wavelength can be determined from the oscillation in the backscattered yield as a function of depth. Thus the catastrophic dechanneling condition is determined experimentally by varying the beam energy until the distance between the planar channeling oscillation peaks, which is one-half the effective wave length, equals the layer thickness in the superlattice. It is not obvious, of course, that this gives the maximum rate of dechanneling, but it should be close. Our initial work on catastrophic dechanneling is reported in Refs. 1 and 2 and more details will follow in two forthcoming papers.[22,23]

C. Resonance channeling

In Fig. 6 we show the case $\theta=2\pi(\lambda_e=s)$, which is the case which maximizes the channeled fraction. Here we have the same initial configuration as in Fig. 5, however, the particles rotate through an angle 2π in each layer. Thus in each layer they come back to their original phase coordinates. In the example of Fig. 6 the particles start at $\psi_0=(\Delta/\psi)/2$, rotate through 2π, and move under the impulse to $-(\Delta\psi)/2$. They then rotate through 2π back to $-(\Delta\psi)/2$ and then move under the impulse to $(\Delta\psi)/2$. Thus the particles' transverse momenta oscillate between $(\Delta\psi)/2$ and $-(\Delta\psi)/2$ at successive interfaces and dechanneling takes place only in the first layer. Thus

every initial condition gives rise to a periodic motion of period $2s$, and this case will be important in our discussion of resonance in the nonlinear model. The MHM therefore suggests this as a second interesting case to investigate both theoretically in the full Moliere model and experimentally. Our experimental discussion of this case will be the subject of a forthcoming paper.[24]

V. PHASE FLOW AND DEPTH DEPENDENCE OF RESONANCE PHENOMENON

The definition of the two resonance phenomena in the MHM and the experimental determination of the energy for catastrophic dechanneling is clear. Furthermore, since the wavelength is proportional (approximately)[34] to the square root of the energy, the resonance channeling energy should be approximately one-fourth of the catastrophic dechanneling energy. However, more exact potentials require a nonlinear model [Eq. (16)] and the definitions of maximal dechanneling and channeling are not so simple. We postpone our discussion of this problem and its partial solution until the next section. Here we take the values as determined by experiment and then see what the nonlinear model with the Moliere potential predicts. We take the case $s=444$ Å, $\Delta\psi=0.15°$, and $x_c=d_p/2-a_T$. The experimentally determined value of the energy for catastrophic dechanneling is 1.2 MeV and thus the energy for resonance channeling is 0.3 MeV. We use the phase flow as shown in Figs. 8–10 to illustrate two cases with $E=1.2$ MeV and one case with $E=0.3$ MeV using the static Moliere potential. In the process we examine the depth dependence of the dechanneling and compare the results with the MHM.

Figure 8 shows the calculated phase flow and associated trajectories for a catastrophic dechanneling case in both the full model and the MHM. Here $E=1.2$ MeV and from Eq. (13) $\psi_c=0.338°$. We integrate Eq. (16) numerically for 200 particles uniformly distributed in $(-d_p/2, d_p/2)$ as shown by the horizontal line labeled 0 in the first phase flow diagram on the right side of Fig. 8. Initially, there are two groups of particles with transverse energy $E_\perp \geq E_{\perp c}$. The first group has $|x| \geq x_c$, and these are taken to be dechanneled immediately. The second group has $E_\perp > E_{\perp c}$ but $|x| < x_c$, and these are dechanneled in the first layer as their clockwise rotation on the integral curves [defined by Eq. (9)] carry them to $x=x_c$. Those particles with $x_0>0$ reach $x=x_c$ first whereas after some delay those with $x_0<0$ reach $x=x_c$. The dechanneled fraction as a function of depth is shown in Fig. 11 by the solid line for catastrophic dechanneling. Since the fraction of particles in the second group mentioned above is quite small, for this example, one observes in Fig. 11 only a constant dechanneled fraction in the first layer of about 0.15, which corresponds to the initially dechanneled fraction $|x| > x_c = dp/2 - a_T$.

The phase flow has taken the initial horizontal line to the curved solid line at the first interface as shown on the right side of Fig. 8. Because the particles that started with $E_\perp \geq E_{\perp c}$ have been dechanneled in the first layer, all particles on the solid line have transverse energies less than $E_{\perp c}$. At the interface this solid line is moved down $\Delta\psi$ to the dashed line in Fig. 8 and now some of the parti-

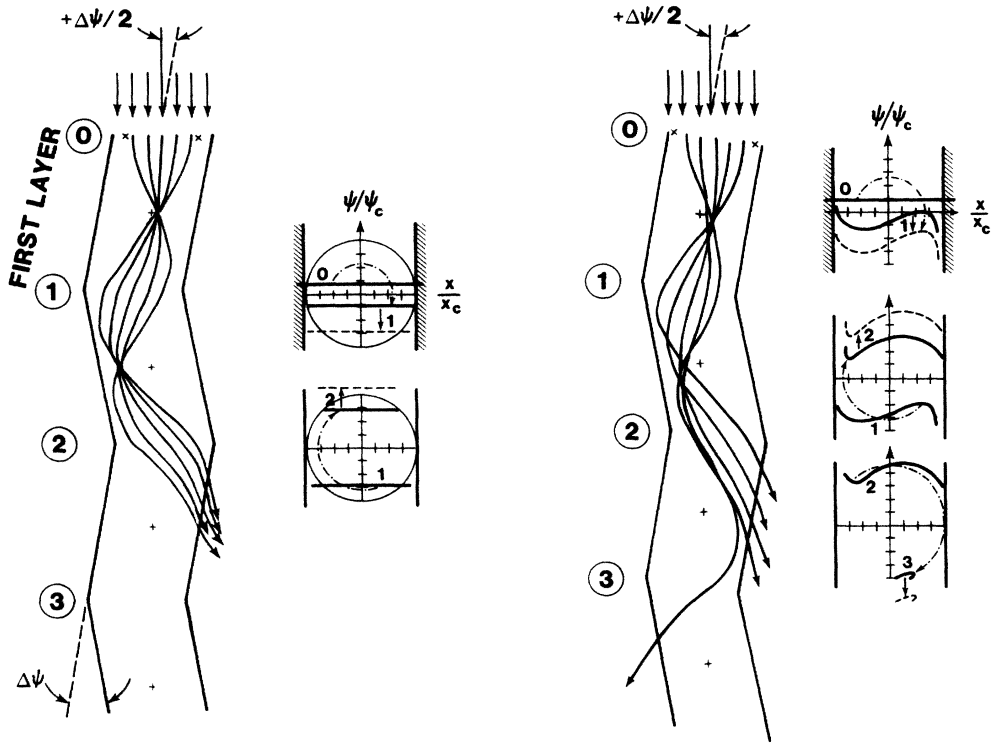

FIG. 8. Phase flow and trajectory calculation for the catastrophic case based on (a) MHM and (b) Moliere potential. The incident angle is $+\Delta\psi/2$ and $E=1.2$ MeV. The solid heavy vertical lines correspond to $x/x_c=1$.

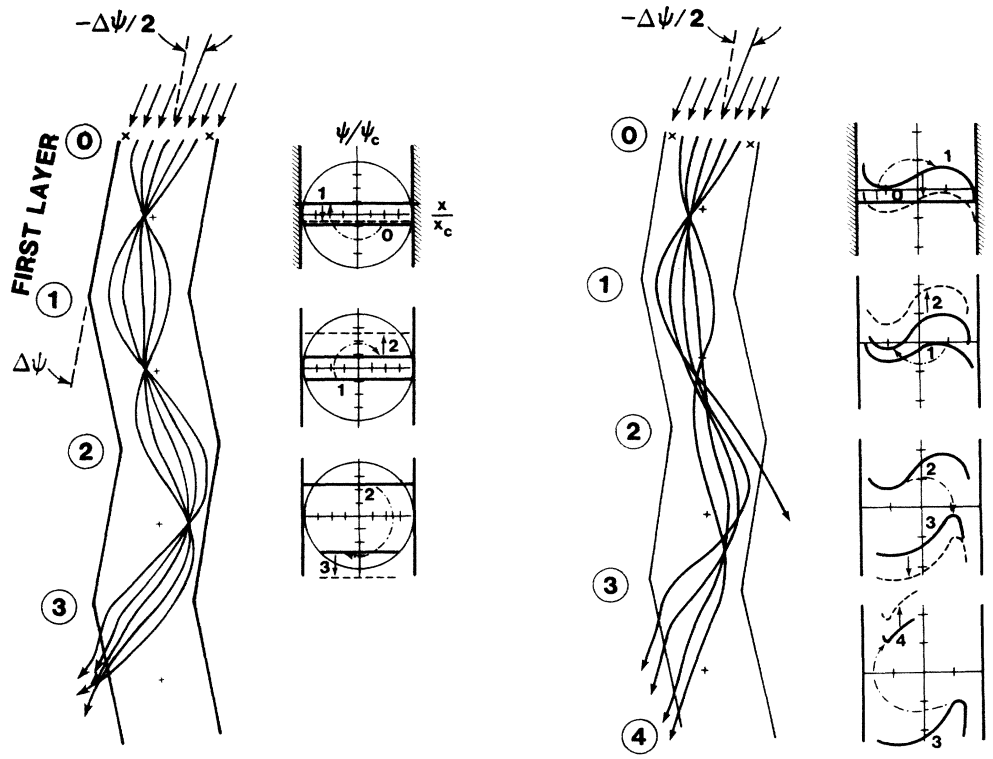

FIG. 9. Same as Fig. 8, except the incident angle is $-(\Delta\psi)/2$. One can see the delay of the catastrophic dechanneling depth by exactly one layer thickness for the MHM and approximately one layer thickness for steering by a static Moliere continuum potential.

cles have transverse energy greater than $E_{\perp c}$. This line is shown by the lower solid line in the phase flow diagram for the second layer. There are now two new groups of particles with $E_\perp \geq E_{\perp c}$ and these are at the two ends of the solid line. As this line moves under the flow, the group on the left will reach $x=-x_c$ first and become dechanneled followed by the group on the right. This gives the two-step structure in layer two (between interface 1 and 2) as shown in Fig. 11. The phase flow curve just before the second interface is shown by the upper solid line. This line moves up $\Delta\psi$ as it crosses the second interface and is shown by the dashed line.

The dashed phase flow line shown in the second diagram is replaced by the solid line in the upper part of the third-phase flow diagram in Fig. 8. This line has two groups of particles with $E_\perp \geq E_{\perp c}$, a large group on the right end and a small group at the left end. As these particles move into the plane at $x=x_c$ they will become dechanneled. The first group gives rise to the large increase in the dechanneled level of Fig. 11 between depths 2 and 2.5; the second group begins to be dechanneled near 2.5 while the first group is still being dechanneled. This is the reason there is no flat region in layer three of Fig. 11 until both groups are totally dechanneled near the end of the layer. There is a small segment remaining at the end of layer three and this moves to the dashed line as they cross the third interface. All the particles now have $E_\perp \geq E_{\perp c}$ and will be dechanneled in the fourth layer as shown in Fig. 11. In studying the phase flow of, for example, Fig. 8, it should be noted that the particles are only uniformly distributed on the phase flow line in the initial state.

The phase flow for the MHM, shown on the left side of Fig. 8, follows the full model (right side) in an average way. This similarity is the reason for the qualitative agreement between the two models shown in Fig. 11 for the depth dependence of the dechanneled fraction. The lack of agreement near interface 3 can be understood from the phase flow of Fig. 8 where it is seen that in the MHM all particles become dechanneled in layer 3.

The dechanneled fraction as a function of depth is easily calculated in the MHM. Here we derive the formula for the dechanneled fraction at each interface under catastrophic dechanneling conditions. Let x_0, ψ_0 denote the initial condition of a particle in layer one. Then the initial condition for the particle's motion in the nth layer is x_0^n, ψ_0^n, where

$$x_0^n = (-1)^{n-1} x_0$$

and

$$\psi_0^n = (-1)^{n-1}[\psi_0 + (n-1)\Delta\psi] \ .$$

Therefore the motion in the nth layer is given by Eq. (15) with x_0, ψ_0 replaced by x_0^n, ψ_0^n, and z going from 0 to s in that layer, that is

$$\frac{x(z)}{x_c} = \frac{x_0^n}{x_c}\cos\left[\frac{2\pi}{\lambda_e}z\right] + \frac{\psi_0^n}{\psi_c}\sin\left[\frac{2\pi}{\lambda_e}z\right] , \tag{21a}$$

$$\frac{\psi(z)}{\psi_c} = -\frac{x_0^n}{x_c}\sin\left[\frac{2\pi}{\lambda_e}z\right] + \frac{\psi_0^n}{\psi_c}\cos\left[\frac{2\pi}{\lambda_e}z\right] . \quad (21b)$$

Clearly a particle is dechanneled in layer n if it has not been dechanneled in layers $1,\ldots,n-1$ and then reaches a condition corresponding to being dechanneled in layer n, that is, $(x_0/x_c)^2+(\psi_0^k/\psi_c)^2$ is less than 1 for $1\le k<n$ and greater than or equal to one for $k=n$. If a particle is dechanneled in layer n, it is a simple matter, using Eq. (21a), to find the depth in that layer for which it is dechanneled. This is the method used to find the dechanneling (dashed line) in the MHM shown in Fig. 11. It is considerably faster than finding the corresponding curve for the full model. It is easy to see that the portion of the line still inside the circle $(x/x_c)^2+(\psi/\psi_c)^2=1$ just before the nth interface corresponds to the channeled fraction $1-\chi(n)$ at the nth interface, giving

$$1-\chi(n)=\begin{cases}\dfrac{2x_c}{dp}\left[1-\left[\dfrac{\psi_0}{\psi_c}\right]^2\right]^{1/2}, & n\le 1-\dfrac{2\psi_0}{\Delta\psi} \text{ and } \left|\dfrac{\psi_0}{\psi_c}\right|\le 1 ,\\ \dfrac{2x_c}{dp}\left[1-\left[\dfrac{\psi_0^n}{\psi_c}\right]^2\right]^{1/2}, & n>1-\dfrac{2\psi_0}{\Delta\psi} \text{ and } \left|\dfrac{\psi_0^n}{\psi_c}\right|\le 1 ,\\ 0, & \left|\dfrac{\psi_0}{\psi_c}\right|>1 \text{ or } \left|\dfrac{\psi_0^n}{\psi_c}\right|>1 .\end{cases} \quad (22)$$

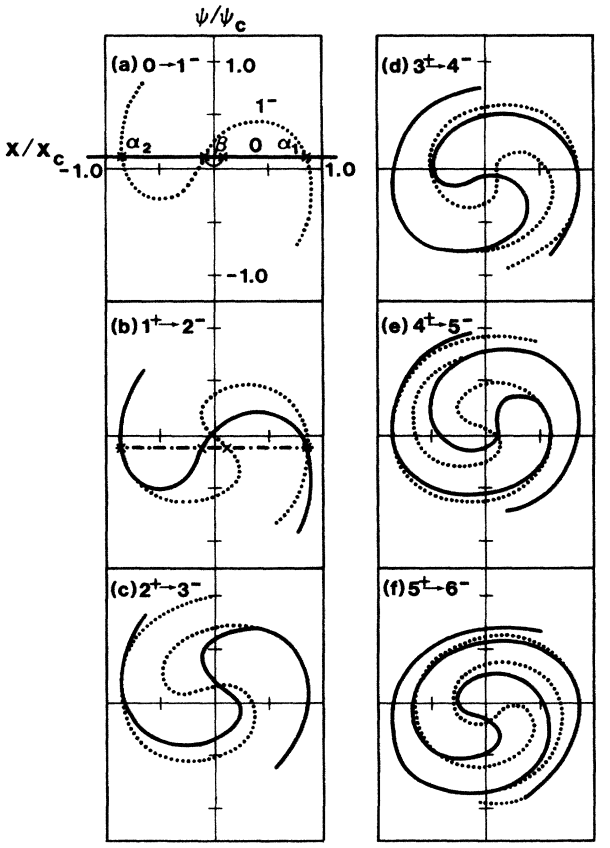

FIG. 10. Phase flow for the resonant channeling case of $E=0.3$ MeV calculated for steering of projectile trajectories by a static Moliere continuum potential. The sequence of phase flow portraits (a)–(f) shows phase flow just before (dashed line labeled $-$) and after (solid line labeled $+$) crossing the layer interfaces of layers 1–6, respectively. The parameter values are $s=444$ Å, $x_c=dp/2-a_T$, $\Delta\psi=0.15°$, and $\psi_0=(\Delta\psi)/2$.

Notice that for $\psi_0=0$ the channeled fraction at the first interface is $2x_c/d_p$ and that if ψ_0 is negative then it is possible for the dechanneled fraction to remain constant over several layers. For the example of Fig. 8, $x_c=0.829$ Å, $\psi_c=0.338°$, $\psi_0=0.075°$, and $\Delta\psi=0.15°$, so that for $n=2$, $|\psi_0^n/\psi_c|=0.666$ and $\chi(2)=0.36$, which is in agreement with Fig. 11.

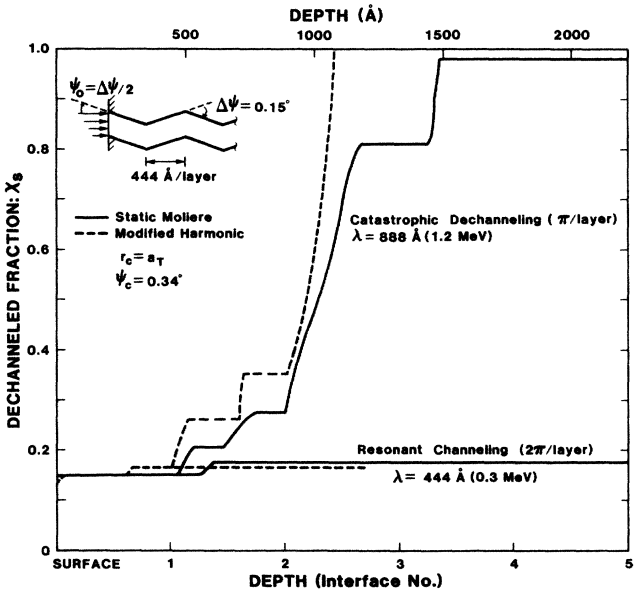

FIG. 11. Calculation of dechanneling vs depth for SLS layers. At 1.2 MeV where $\lambda_e/2=444$ Å (path length per layer), *catastrophic dechanneling* occurs and maximum dechanneling is observed. At 0.3 MeV, where $\lambda_e=444$ Å, *resonance channeling* occurs and minimum dechanneling is observed. Calculations are based on the static Moliere continuum potential (solid lines) and the modified harmonic model (dashed lines) for an incident angle of $(\Delta\psi)/2$.

Figure 9 shows the corresponding phase flow for the catastrophic dechanneling case with $\psi_0=-\Delta\psi/2$. This corresponds to shifting the incident angle by the superlattice title angle $-\Delta\psi$ and by comparison with Fig. 8 it can be seen that this change delays the catastrophic dechanneling by one layer in the MHM and by approximately one layer in the full model. The consequence of this connection between incident angle and catastrophic dechanneling depth for strain measurements will be discussed in Sec. VII.

Figure 10 shows the calculated phase flow for the resonance channeling case of $E=0.3$ MeV, which gives $\psi_c=0.676°$. As in the case of Figs. 8 and 9, Eq. (16) has been integrated numerically for 200 particles uniformly distributed in $(-d_p/2,d_p/2)$ as shown by the horizontal line in Fig. 10(a). In Fig. 10(a) the phase flow has taken the horizontal line to the curved dotted line labeled 1^- just before the first interface. The phase flow curve has returned to its initial position in an average way, whereas in the resonance channeling case of Fig. 6 for the MHM it has exactly returned to its initial position. The three points, α_1, α_2, and β, where the two-phase flow curves cross in Fig. 10(a) are important. They are related to periodic solutions of Eq. (16) and will be discussed shortly. The solid phase flow curve in 10(b) is the dotted curve of 10(a) moved down $\Delta\psi$, and it evolves to the dotted curve upon passing through layer 2. Notice how all the particles are staying in the channeled particle portion of the phase portrait. The solid phase curve in 10(c) is the dotted curve of 10(b) moved up $\Delta\psi$, and it evolves to the dotted curve in layer 3. This procedure is followed in layers 4, 5, and 6 as shown in the figure, and the important thing to observe is that the spirals, which are becoming wound tighter and tighter, are staying in the center of the portrait indicating very little dechanneling. This is verified by the calculation of the dechanneled fraction which is shown in Fig. 11. Here it is seen that there is an initial dechanneled level which is maintained through layer 1, a small amount of dechanneling in layer 2, and then no dechanneling through layer 5. The calculation has been carried through 10 layers, over which no additional dechanneling has occurred. Even though the phase flows for the MHM and the full model appear very different, their predictions of the dechanneled fraction are in agreement.

To help understand the phase flows of Fig. 10 and the small amount of dechanneling, we will follow the particles labeled α_1, α_2, and β on the horizontal line of Fig. 10(a). If we let (x_0,ψ_0) denote the initial coordinates of α_1, then α_1 moves back to its initial position as it moves through the first layer. At the interface it moves down $\Delta\psi$ to $(x_0,-\psi_0)$ and then in layer 2 it moves back to $(x_0,-\psi_0)$ as it approaches the second interface. At the second interface it moves up $\Delta\psi$ to (x_0,ψ_0) and it is now back to its entrance conditions for layer 1. Since the superlattice structure repeats itself every two layers [the right-hand side of Eq. (16) has period $2s$], the particle α_1 has periodic motion. The same argument works for α_2. Thus the initial conditions for α_1 and α_2 give rise to periodic solutions of Eq. (16) with the period of the SLS. These motions, as shown in Figs. 10(a) and 10(b) are partially responsible for the small amount of dechanneling, just as in the case of the MHM of Fig. 6, where all motions starting on the horizontal line of Fig. 6 are periodic, and this allows no dechanneling after the first one or two layers. The particle labeled β also corresponds to a periodic solution as will be discussed in Sec. VI.

In summary, Fig. 11 shows that the resonance effects predicted by the MHM are corroborated by the full model. There is clearly a big difference between the depth dependence of the dechanneled fraction for the two cases, $E=1.2$ MeV and $E=0.3$ MeV. While it is clear how to give a precise definition of resonance in the MHM, it is not so clear in either the experimental situation or in the full nonlinear model. Theoretical aspects of this problem will be discussed in the next section.

VI. FURTHER DISCUSSIONS ON RESONANCE

It is important to understand the conditions which give the maximum rate of dechanneling and the maximum channeling. A rough estimate of this can be found by defining an effective channeled particle wavelength λ_e which depends on the beam energy and other channeling parameters. The catastrophic dechanneling condition is then $\lambda_e\approx 2s$ and the resonant channeling condition is then $\lambda_e\approx s$. Experimentally, λ_e is determined from the oscillations in the backscattered yield, while theoretically it can be determined from calculations which produce the wavelength as a function of amplitude as shown in Fig. 2. A reasonable λ_e would be the wavelength associated with amplitude $d_p/2-a_T$, corresponding to $A\simeq 0.86$ in Fig. 2. The other extreme is to carry out extensive numerical and experimental work to try to determine the maximal dechanneling and transmission. From a theoretical point of view neither of these is particularly satisfying, and here we suggest an approach which, when combined with numerical experiments, may illuminate the problem.

Attempts to analytically characterize the maximum rate of dechanneling for the nonlinear case were not successful and so we focused instead on the resonance channeling problem of finding conditions for which particles remain in the channeled phase space region. Clearly the simplest such situation occurs for periodic motions, and so a study of periodic solutions of Eq. (16) was initiated. This study is still in its preliminary stages, and here we report on a special case which we believe contains the seed for a full understanding of resonance channeling. Indirectly, this illuminates the catastrophic dechanneling since those effects occur at roughly four times the energy associated with the resonance channeling.

We assume s and $\Delta\psi$ are given in Eq. (16) and consider initial conditions on the line $\psi(0)=\psi_0=(\Delta\psi)/2$. It should be clear from Eq. (10) that there exists an energy, position pair E,η, with $0\le\eta<x_c$, such that $\lambda(E_\perp)=s$, where $E_\perp=E\psi_0^2+U(\eta)$, that is

$$s=\lambda(E_\perp):=4\sqrt{E}\int_0^a[U(a)-U(x)]^{-1/2}dx\ , \qquad (23)$$

where a and $U(a)$ are defined by $U(a)=E\psi_0^2+U(\eta)$. The phase plane position $(x,\psi)_z$ at z of the particle starting at (η,ψ_0) with this value of E evolves as follows:

$$(x,\psi)_0=(\eta,\psi_0)\rightarrow(x,\psi)_{s^-}=(\eta,\psi_0)\rightarrow(x,\psi)_{s^+}=(\eta,-\psi_0)\rightarrow(x,\psi)_{2s^-}=(\eta,-\psi_0)\rightarrow(x,\psi)_{2s^+}=(\eta,\psi_0)\ .$$

Thus this initial condition with $E=E(\eta)$ gives rise to a periodic solution of Eq. (16), with $E(\eta)$ defined by Eq. (23), as discussed in Sec. IV for the particle labeled α_1 in Fig. 10.

By symmetry the initial condition $(-\eta,\psi_0)$ also leads to a periodic solution. These periodic solutions exist for the range of energies $E(0)\le E\le E(x_c)$ (from the calculation which produced Fig. 10 we know that $\eta\simeq 0.86x_c$ so that $E(0.86x_c)\cong 0.30$ MeV, and this gives an interval of possible energy values for the maximum channeling condition which we call the resonant channeling interval. Clearly the existence of these periodic solutions has the effect of holding the phase flow curve in the channeling region at least for small distances into the crystal. Also the stability and position η of these periodic solutions are relevant and will control the "holding power." The problem is then to find the η in $[0,x_c]$ which has the greatest holding power. Before making these ideas more concrete we point out that for every E,η pair giving rise to the two periodic solutions there exists an $\xi(\eta)$ such that $0\le\xi\le\eta$ and the initial conditions $(\xi,\ \Delta\psi/2)$ also give rise to a periodic solutions. To see this, let $(-\eta,\psi_0)$, $(-\xi,\psi_0)$, and (η,ψ_0) denote the points of intersection of the phase flow curves at $z=0$ and $z=s$ as seen for example in Figs. 10(a). We have already shown that the point (η,ψ_0) on the phase flow curve at $z=s$ came from the same point at $z=0$, that is, $s=\lambda(E_\perp)=\lambda(E\psi_0^2+U(\eta))$. Because of conservation of transverse energy the point $(-\xi,\psi_0)$ at $z=s$ could only have come from (ξ,ψ_0) or $(-\xi,\psi_0)$ at $z=0$ and because λ is a monotone decreasing function of $E_\perp$ it must have come from (ξ,ψ_0). Therefore, the point (ξ,ψ_0) at $z=0$ moves to $(-\xi,\psi_0)$ at $z=s^-$ under the flow and then moves to $(-\xi,-\psi_0)$ at $z=s^+$ after crossing the first interface. Because the integral curves are symmetric about the x and ψ axes, the point at $(-\xi,-\psi_0)$ at $z=s^+$ moves to $(\xi,-\psi_0)$ at $z=2s^-$ under the flow and then moves to (ξ,ψ_0) at $z=2s^+$ after crossing the second interface. That is, the point (ξ,ψ_0) returns to its original position at $z=2s^+$ and since the SLS structure has period $2s$ the particle motion repeats and we have another periodic solution of Eq. (16). Thus we actually have three periodic solutions of period $2s$ helping to hold the phase flow in the channeling region.

It seems likely that for η small the large tails of the phase flow curve could easily become dechanneled. Furthermore, if η is too large, this particle could become dechanneled leaving only one periodic orbit to contain the phase flow. Based on this and our experience with the numerical calculations, we suspect the best holding power will occur for $\eta\approx\frac{3}{4}x_c$ and propose this as a resonance channeling condition.

In order to better understand the E,η relation and in order to obtain a simple estimate for the resonance channeling energy interval, we introduce the tangent square potential $U(x)=b\tan^2(ax)$, which gives a very good approximation to the Moliere potential.[18] This potential is convenient because Eq. (10) gives

$$\lambda(E_\perp)=\frac{2\pi}{a}\left[\frac{E/b}{1+(E_\perp/b)}\right]^{1/2}$$

and since

$$E_\perp=E\left[\frac{\Delta\psi}{2}\right]^2+b\tan^2(a\eta)\ ,$$

Eq. (23) can be solved for E giving

$$E(\eta)=\frac{1}{\cos^2(a\eta)}\left[\frac{\left[\frac{sa}{2\pi}\right]^2 b}{1-\left[\frac{sa\ \Delta\psi}{4\pi}\right]^2}\right]\ . \tag{24}$$

Thus, the dependence of E on η is easily understood. To find a and b we require that the tangent square and Moliere wavelength functions match for $E_\perp=0$ and $E_\perp=U[0.8(d_p/2)]$; this is discussed in detail in Ref. 18. From Fig. 2 these values are 1115 Å and 844 Å giving $a=0.92(\text{Å})^{-1}$ and $b=45.0$ eV. For $\eta=0.75x_c$ we obtain $E=0.27$ MeV and for $\eta=0.86x_c$ we obtain $E=0.30$ MeV consistent with our experimentally determined resonance channeling energy of $E=0.3$ MeV.

It is hoped that the reader now has some feel for this situation and that Eq. (24) is a handy formula for quickly estimating the resonance channeling interval. Furthermore, with our conjecture of $\eta\approx\frac{3}{4}x_c$ having the greatest holding power we obtain a simple formula for estimating the resonant channeling energy from Eq. (24) and the catastrophic dechanneling energy is a factor of 4 larger.

VII. INCIDENT ANGLE DEPENDENCE OF CATASTROPHIC DECHANNELING

The resonance phenomena presented in Secs. IV and V were discussed for the fixed incident angle $\psi_0=+(\Delta\psi)/2$. In this section, we consider the incident angle dependence of the channeling at resonance. In the MHM of Figs. 5 and 6, a change in initial angle corresponds to a change in the position of the horizontal line labeled O. For larger ψ_0, the line will be higher, and for negative ψ_0, the line will be below the x axis. For resonance channeling in the MHM it is easy to see from Fig. 6, that a change in the initial angle will only shift the relative position of the two horizontal lines on the ψ/ψ_c axis. Thus the particles will still oscillate between the two angular positions ψ_0 and $\psi_0-\Delta\psi$ and no dechanneling will occur after the first two layers. The dechanneled fraction χ_R after this initial dechanneling will be

$$\chi_R=\max_{i=0,1}\left\{1-\frac{2x_c}{d_p}\left[1-\left[\frac{\psi_0-i\ \Delta\psi}{\psi_c}\right]^2\right]^{1/2}\right\} \tag{25}$$

as long as $|\psi_0|$ and $|\psi_0-\Delta\psi|$ are less than ψ_c. The angular dependence of resonance channeling is therefore easy to understand in the MHM, and we will not ela-

borate further here.

In contrast to the resonant channeling case, the catastrophic dechanneling resonance condition leads to a much more dramatic dependence on incident angle. In the MHM, it is easy to see that reducing the incident direction ψ_0 by $\Delta\psi$ delays the depth of the catastrophic dechanneling by one layer. This is because immediately after the first-layer rotation by π the incident beam direction at the first interface becomes $-(\psi_0-\Delta\psi)-\Delta\psi = -\psi_0$. But for dechanneling considerations entering the first interface with angle $-\psi_0$ are identical, by symmetry, to entering the surface at ψ_0. The left-hand side of Figs. 8 and 9 clearly show this behavior in the case of $\psi_0=\Delta\psi/2$ and $\psi_0=-\Delta\psi/2$. If we let $D_c(\psi_0)$ denote the depth of catastrophic dechanneling (for example, the depth at which 85% of the particles are dechanneled), then $D_c(\psi_0)-D_c(\psi_0-\Delta\psi)=-1$ and hence $\Delta D_c(\psi_0)/\Delta\psi = -1/\Delta\psi$. Thus the depth of catastrophic dechanneling versus incident angle should have an "average" slope of $-1/\Delta\psi$ and thus be a measure of the strain $\Delta\psi$.

In Fig. 12 we show the depth for 85% dechanneling in the catastrophic dechanneling case. The solid line is based on the full model calculations for the static Moliere potential as discussed previously. A detailed step structure is predicted and this structure contains both strain and potential information.

The dashed line in Fig. 12 represents the MHM and is easily computed from Eq. (21). It agrees well with the full model for the choice of parameters here in spite of the fact that the detailed phase flows for the two cases are different. This reflects the fact that the phase flow in the MHM follows in an average way the phase flow of the full model. The jump discontinuities occur across the interfaces $n=1$, 2, 3, 4, and 5, at values of $\psi_0=\psi_0(n)$ such that

$$\psi_0(n)=\psi_c A-(n-1)\Delta\psi\ , \tag{26}$$

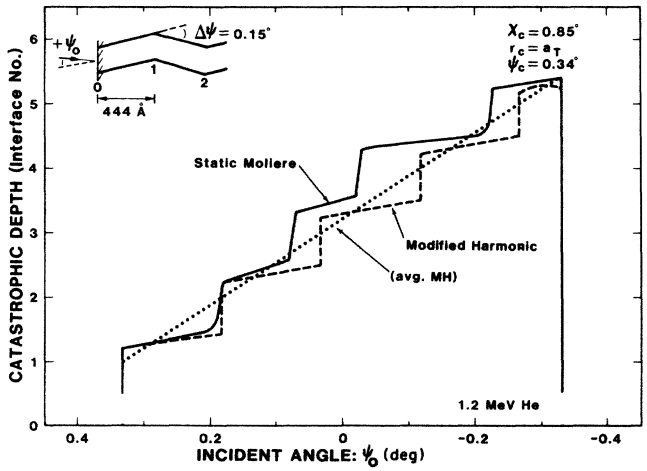

FIG. 12. Calculation of catastrophic dechanneling depth as a function of incident angle for a static Moliere continuum potential (solid line), the MHM (dashed line), and the average MHM (dotted line). The observed angular dependence is highly anisotropic.

where

$$A=\{1-[(1-\chi_c)d_p/2x_c]^2\}^{1/2}$$

for $\chi_c=0.85$, $A=0.985$. Equation (22) gives the dechanneled fraction at the nth interface as a function of ψ_0; however, it also can be used to determine $\psi_0=\psi_0(n)$ such that the dechanneled fraction at the nth interface is given by $\chi(n)=\chi_c$. This yields Eq. (26). To understand the jump discontinuity notice that $\psi_0(2)=0.183°$. This jump is due to the existence of a group of particles which for $\psi_0\gtrsim 0.183°$ are dechanneled in the second layer but for $\psi_0\lesssim 0.183°$ are dechanneled in the third layer. The points $[n,\psi_0(n)]$ defined by Eq. (26) lie on a straight line with slope $-1/\Delta\psi$ as shown by the dotted line in Fig. 12. This gives a reasonable average for the full MHM calculation where the particles are counted as dechanneled as they rotate into the planes. Equation (26) also clearly shows that the catastrophic depth is delayed by one layer for a $\Delta\psi$ decrease in ψ_0 since $\psi_0(n+1)=\psi_0(n)-\Delta\psi$. The fact that the slope of this line (average MH in Fig. 12) is simply related to the strain and that this line has a slope fairly close to the average slope of the full model gives a quick method for estimating the strain from experimental data.

VIII. SCALING LAWS

Here we investigate the scaling laws in the full model and present a set of universal curves for the dechanneled fraction as a function of depth in the catastrophic dechanneling case.

The equation of motion given by Eq. (16) becomes

$$\frac{d^2X}{dZ^2}+\Omega^2W'(X,D)=\sum(-1)^j\Delta\Psi\,\delta(Z-j) \tag{27}$$

under the scaling

$$X=\frac{x}{d_p/2},\quad Z=\frac{z}{s},\quad U(x)=KW(X,D) \tag{28}$$

for $K=\pi z_1z_2e^2Nd_p^2$ and $D=d_p/a_T$, where

$$\Omega^2=\frac{1}{2}\frac{K}{E}\left[\frac{2s}{d_p}\right]^2 \text{ and } \Delta\Psi=\frac{s\,\Delta\psi}{d_p/2}\ . \tag{29}$$

If we introduce the geometrical angle $\psi_g=(d_p/2)/s$ and note that $E\psi_p^2=(2/D)K$, then Ω and $\Delta\Psi$ can be rewritten as

$$\Omega^2=\frac{D}{4}\left[\frac{\psi_p}{\psi_g}\right]^2 \text{ and } \Delta\Psi=\frac{\Delta\psi}{\psi_g}\ .$$

For the case of this paper $D=14.06$ and $\psi_g=0.125°$. Because a particle becomes dechanneled when $X=X_c$, the fraction of channeled particles at a fixed Z depends only on Ω, $\Delta\Psi$, and D for a given initial angle Ψ_0. For crystals of interest, the sensitivity to D is very small. Furthermore, Ω has a particular value for a resonance condition, e.g., $\Omega\approx 5.96$ here for catastrophic dechanneling. Thus given the resonance condition, an average D value, and an initial particle ensemble, we can construct a set of universal curves for the dechanneled fraction versus Z for various values of the normalized interface tilt angle $\Delta\Psi$.

A set of universal curves of the dechanneling versus depth based on the scaling for Eqs. (28) and (29) are shown in Fig. 13 for the resonance case of catastrophic dechanneling and incident beam direction $\psi_0=0$. The curves show the evolution from no catastrophic dechanneling for normalized SLS tilt angle $\Delta\Psi=0$ to total dechanneling in the second layer for $\Delta\Psi=140$. The increase in catastrophic dechanneling with tilt angle is seen to occur by the smooth increase in the dechanneled step heights in the layers and incremental movement to succeedingly shallower layers. The solid lines of Fig. 13 are calculated for the standard case used in this paper of He along the {110} planes with average spacing for the SLS $GaAs_{0.15}P_{0.85}/GaP$, which corresponds to a normalized planar spacing of $D=14.06$. For the case of $\Delta\Psi=80$ we also show for comparison the dechanneling versus depth (dashed line) for $D=15.54$ which corresponds to the $GaAs_{0.8}P_{0.2}/GaAs$ ($d_p\simeq 2$ and $a_T=0.1287$ Å) studied in a forthcoming paper.[24] This range of D values roughly represents the range of planar spacings to be found in groups IV and III–V SLS materials. Thus the dependence of planar spacing is weak and the plot of Fig. 13 represents a useful set of universal curves for predicting the rate of catastrophic dechanneling at $\psi_0=0$ for any given strained-layer superlattice of equal layer thickness. Equation (27) could equally well be utilized to obtain universal curves for any other resonance condition or with appropriate modification for any other SLS structure.

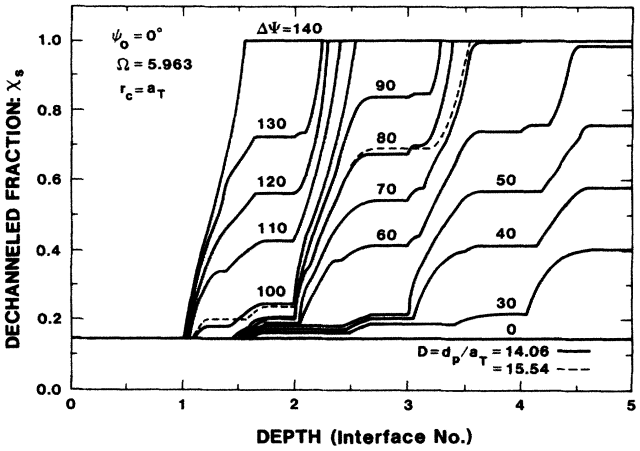

FIG. 13. Universal curves of the depth dependence of catastrophic dechanneling calculated for a static Moliere continuum potential. These curves can be used to predict the layer strains for an arbitrary strained-layer superlattice with equal thickness layers. The solid lines correspond to the $GaAs_{0.15}P_{0.85}/GaP$ case of this paper ($D=14.06$) and the dashed line for $\Delta\Psi=80$ corresponds to the case of $GaAs_{0.85}P_{0.15}/GaAs$ SLS ($D=15.54$).

IX. CONCLUSIONS

In conclusion we have developed the continuum theory of channeling for layered crystalline structures and applied it to superlattices. Because these structures are in the surface region, energy loss and multiple scattering can to first order be ignored. The model is a one-degree-of-freedom nonlinear oscillator forced with a periodic delta function with alternating impulses, an equation of current mathematical interest. Because the natural periods are close to the forcing periods for MeV channeling in SLS's of current interest, resonance effects are to be expected and we have explored two of these effects in detail. In the nonlinear model the resonance channeling (minimum dechanneling) is easier to define than catastrophic dechanneling because of the existence of periodic solutions of Eq. (16). Also, a simple linear model is used to explain the relation between the two resonance conditions. We compared our nonlinear model with our previous MHM, which is basically a linear resonance model, and found good agreement. This agreement results because the phase flow in the MHM follows the nonlinear phase flow in an average way for the shallow depths of interest. We gave a detailed discussion of the depth dependence of the dechanneling for both resonance conditions in terms of the phase flow (Figs. 8–10) and used this to explain the depth profile of the catastrophic dechanneling (Fig. 11). A set of nearly universal curves for the depth profile of catastrophic dechanneling was presented. Finally, the incident angle dependence of the catastrophic dechanneling was discussed in both the nonlinear model and the previous MHM.

ACKNOWLEDGMENTS

One of us (J.A.E.) was supported by the National Science Foundation under Grant No. DMR-82-14301. Three of us (S.T.P, W.R.A., and W.K.C.) were supported by the U.S. Department of Energy under Contract No. DE-AC04-76DP00789.

[1]W. K. Chu, J. A. Ellison, S. T. Picraux, R.M. Biefeld, and G. C. Osbourn, Phys. Rev. Lett. **52**, 125 (1984).
[2]S. T. Picraux, W. R. Allen, R. M. Biefeld, J. A. Ellison, and W. K. Chu, Phys. Rev. Lett. **54**, 2355 (1985).
[3]W. K. Chu, W. R. Allen, J. A. Ellison, and S. T. Picraux, Nucl. Instrum. Methods B **13**, 39 (1986).
[4]S. T. Picraux, L. R. Dawson, G. C. Osbourn, and W. K. Chu, Appl. Phys. Lett. **43**, 930 (1983).
[5]S. T. Picraux, L. R. Dawson, G. C. Osbourn, R. M. Biefeld, and W. K. Chu, Appl. Phys. Lett. **43**, 1020 (1983).
[6]C. K. Pan, D. C. Zheng, T. G. Finstad, W. K. Chu, V. S. Speriosu, and M. A. Nicolet, and J. H. Barrett, Phys. Rev. B **31**, 1270 (1985).
[7]J. H. Barrett, Phys. Rev. B **28**, 2328 (1983).

[8]W. K. Chu, F. W. Saris, C. A. Chang, R. Ludeke, and L. Esaki, Phys. Rev. B **26**, 1999 (1982).
[9]W. K. Chu, C. K. Pan, and C. A. Chang, Phys. Rev. B **28**, 4033 (1983).
[10]J. H. Barrett, Appl. Phys. Lett. **40**, 482 (1983).
[11]S. T. Picraux, L. R. Dawson, G. C. Osbourn, and W. K. Chu, Nucl. Instrum. Methods **218**, 57 (1983).
[12]A. T. Fiory, J. C. Bean, L. C. Feldman, and I. K. Robinson, J. Appl. Phys. **56**, 1227 (1984).
[13]J. C. Bean, L. C. Feldman, A. T. Fiory, S. Nakahara, and I. K. Robinson, J. Vac. Sci. Technol. A **2**, 436 (1984).
[14]S. T. Picraux, W. K. Chu, W. R. Allen, and J. A. Ellison, Nucl. Instrum. Methods B **15**, 306 (1986).
[15]G. C. Osbourn, J. Appl. Phys. **53**, 1586 (1982).
[16]J. Lindhard, Mat. Fys. Medd. Dan. Vid. Selsk. **34**, No. 14 (1965).
[17]D. S. Gemmell, Rev. Mod. Phys. **46**, 129 (1974).
[18]J. A. Ellison, Phys. Rev. B **18**, 5948 (1978).
[19]T. J. Burns and J. A. Ellison, Phys. Rev. B **29**, 2790 (1984).
[20]H. S. Dumas and J. A. Ellison, in *Local and Global Methods of Dynamics,* Vol. 252 of *Lecture Notes in Physics,* edited by R. Cawley, A. W. Sàenz, and W. W. Zachary (Springer-Verlag, Berlin, 1986).
[21]J. A. Ellison and S. T. Picraux, Phys. Lett. **83A**, 271 (1981).
[22]S. T. Picraux, R. M. Biefeld, W. R. Allen, W. K. Chu, and J. A. Ellison (unpublished).
[23]W. K. Chu, W. R. Allen, S. T. Picraux, and J. A. Ellison (unpublished).
[24]W. R. Allen, W. K. Chu, S. T. Picraux, R. M. Biefeld, and J. A. Ellison (unpublished).
[25]P. A. Doyle and P. S. Turner, Acta Crystallogr. Sec. A **24**, 390 (1968).
[26]J. U. Andersen, K. R. Eriksen, and E. Laegsgaard, Phys. Scr. **24**, 588 (1981).
[27]L. D. Landau and E. M. Lifschitz, *Mechanics* (Addison-Wesley, Reading, 1969), pp. 27–29.
[28]W. M. Gibson and J. A. Golovchenko, Phys. Rev. Lett. **28**, 1301 (1972).
[29]J. A. Ellison and T. Guinn, Phys. Rev. B **18**, 5963 (1978).
[30]Equation (3) is integrated numerically using the subroutine RKF45 which is a high-quality subroutine based on Runge-Kutta formulas developed by E. Fehlberg and implemented by L. F. Shampine and H. A. Watts in 1974. It requires six function evaluations per step. Four of these function values are combined with one set of coefficients to produce a fourth-order method, and all six values are combined with another set of coefficients to produce a fifth-order method. Comparison of the two values yields an error estimate which is used for step size control. In our calculations we used absolute and relative errors of 10^{-8}. A discussion and listing of this code can be found in G. E. Forsythe, M. A. Malcolm, and C. B. Moler, *Computer Methods for Mathematical Computations* (Prentice Hall, Englewood Cliffs, 1977), Chap. 6. A similar code is a part of the so-called SLATEC library. For more details see Ref. 31.
[31]W. R. Allen, Ph.D. dissertation, University of North Carolina, Chapel Hill, 1986.
[32]This calculation gives the joint spatial-momentum density $\rho(x,\psi;z)$, but only $\rho(x;z)$ is required for the dechanneling calculation.
[33]J. K. Hale, *Ordinary Differential Equations,* 2nd ed. (Krieger, Florida, 1980), Chap. V; A. J. Lichtenberg and M. A. Lieberman, *Regular and Stochastic Motion* (Springer-Verlag, New York, 1983); J. Guckenheimer and P. Holmes, *Nonlinear Oscillations, Dynamical Systems and Bifurcations of Vector Fields* (Springer-Verlag, New York, 1983).
[34]Equation (10) shows the $\sqrt{E}$ dependence explicitly, however, E can also enter in the $E_\perp$ and a terms. This latter dependency is small.